EPJ Web of Conferences **364**, 05003 (2026) https://doi.org/10.1051/epjconf/202636405003
Quark Matter 2025

Microscopic study of non-Gaussian particle number fluctuations near the critical point

Volodymyr A. Kuznietsov[1,2], Roman Poberezhniuk[1,2], Mark I. Gorenstein[2], Volker Koch[3], and Volodymyr Vovchenko[1]

[1]Physics Department, University of Houston, Houston, TX 77204, USA
[2]Bogolyubov Institute for Theoretical Physics, Kyiv 03680, Ukraine
[3]Lawrence Berkeley National Laboratory, Berkeley, CA 94720, USA

Abstract. We simulate a classical Lennard-Jones fluid at fixed number of particles $N = 400$ via molecular dynamics to study higher-order particle number cumulants near the liquid–gas critical point, along $T = 1.06\,T_c$, at densities $0.32n_c$, $0.95n_c$, and $1.9n_c$. Coordinate space results obtained with a statistics of 2 millions events reveals strong non-Gaussian signals near critical point despite of the suppression due to the baryon number conservation. In momentum space, the cumulants follow ideal gas behavior. Due to collective flow effects imposed the critical signals are partially restored and are especially strong around $\sqrt{s_{\rm NN}} \approx 7.7$ GeV. Our findings are discussed in a context of heavy-ion collision experiments.

1 Introduction

The critical point (CP) of a liquid-gas phase transition leaves an imprint through enhanced fluctuations and long-range correlations. In the context of the QCD, one of the most promising signatures of the CP comes from observing non-Gaussian features in the event-by-event net-proton number distributions measured in heavy-ion collisions [1–3]. To explore these effects in a controlled setting, we turn to molecular dynamics (MD) simulations of a classical Lennard-Jones (LJ) fluid – the system whose critical behavior falls into the 3D-Ising universality class. This microscopic model lets us clearly separate finite-size and conservation-law effects, and, by introducing the Bjorken longitudinal flow, relate the underlying coordinate-space fluctuations to experimentally accessible momentum-space observables.

2 Simulation Setup

2.1 LJ Fluid in MD simulation

We consider a system of $N = 400$ classical particles of mass m evolving under the LJ potential [4, 5],

$$V_{\rm LJ}(r) = 4\epsilon\Big[\big(\tfrac{\sigma}{r}\big)^{12} - \big(\tfrac{\sigma}{r}\big)^{6}\Big]\,.$$

The system temperature and particle number density are expressed in the dimensionless units as $\tilde{T} = T/(\epsilon/k_B)$ and $\tilde{n} = n\sigma^3$, and the reduced time variable is $\tilde{t} = t\sqrt{\epsilon/(m\sigma^2)}$ The CP is at $\tilde{T}_c = 1.321$ and $\tilde{n}_c = 0.316$. We fix the reduced temperature to $\tilde{T} = 1.4 \approx 1.06\,\tilde{T}_c$ and explore

three densities $\tilde{n} = 0.1, 0.3$, and 0.6, corresponding to $0.32\,\tilde{n}_c$, $0.95\,\tilde{n}_c$, and $1.9\,\tilde{n}_c$ respectively. The periodic boundary conditions are enforced in a cubic box of side $\tilde{L} = (N/\tilde{n})^{1/3}$ in micro canonical ensemble with the proper energy per particle to obtain a desired $(\tilde{T}, \tilde{n})$ points. Each run is initialized with random positions and velocities consistent with Maxwell-Bolzmann distribution and integrated using the Velocity–Verlet algorithm [6]. After an equilibration time $\tilde{t} \gtrsim 50$, observables are extracted by averaging over 2 millions independent events to ensure robust statistics for the higher-order cumulants.

2.2 Heavy-Ion Connection

By choosing $N = 400$, we match the typical net baryon number in central Au+Au (or Pb+Pb) collisions. Note that at moderate beam energies the antibaryon yields remain small. This allows us to interpret each MD event as a freeze-out snapshot, with the momentum-space acceptance fraction α directly analogous to the rapidity and transverse-momentum cuts employed in experiments. Global baryon number conservation in our finite system thus mirrors the exact baryon-number constraint in a single heavy-ion collision, enabling quantitative comparisons of cumulants and factorial cumulants with RHIC BES and future FAIR/CBM data.

3 Cumulants and Observables

We measure acceptance-limited particle counts N and define central cumulants $\kappa_k = \langle(\Delta N)^k\rangle$. Key ratios:

$$\omega = \frac{\kappa_2}{\kappa_1}, \quad S\sigma = \frac{\kappa_3}{\kappa_2}, \quad \kappa\sigma^2 = \frac{\kappa_4}{\kappa_2}. \tag{1}$$

Note, that this formulas are not corrected for the global baryon number conservation [7].

4 Factorial Cumulants

To isolate genuine multi-particle correlations, we compute factorial cumulants [8]:

$$\hat{C}_2 = -\langle N\rangle + \kappa_2, \tag{2}$$

$$\hat{C}_3 = 2\langle N\rangle - 3\kappa_2 + \kappa_3, \tag{3}$$

$$\hat{C}_4 = -6\langle N\rangle + 11\kappa_2 - 6\kappa_3 + \kappa_4. \tag{4}$$

These are normalized either as $\hat{C}_k/\langle N\rangle$. In coordinate space at $n = 0.95 n_c$ we find $\hat{C}_3/\langle N\rangle < 0$ and $\hat{C}_4/\langle N\rangle < 0$ with strong non-monotonic dependence on acceptance α. One also could study proton factorial cumulants under isospin randomization and charge conservation, which leads to the additional suppression (see [9]).

5 Coordinate Space Results

In coordinate space, the proximity to the critical density n_c produces non-Gaussian signatures: the kurtosis $\kappa\sigma^2$ exhibits a deep minimum at $\alpha \approx 0.5$ (Fig. 1), while the skewness $S\sigma$ passes through zero as α increases. Furthermore, the factorial cumulants $\hat{C}_3$ and $\hat{C}_4$ amplify the underlying multi-particle correlations, showing non-monotonic dependence on α with extremum near the same acceptance (Fig. 2). Together, these behaviors underscore the enhanced clustering of particles near the CP and validate factorial cumulants as sensitive probes of critical fluctuations in a finite system.

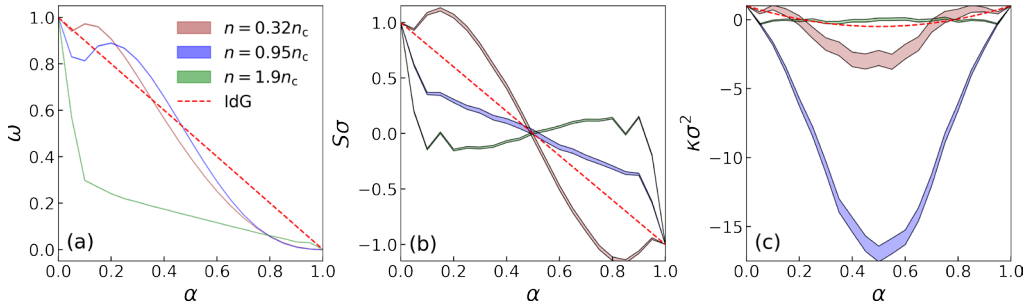

Figure 1. Coordinate-space scaled varience, skewness and kurtosis as a function of acceptance α. Near CP density, $\kappa\sigma^2 \approx -17.5$ at $\alpha = 0.5$.

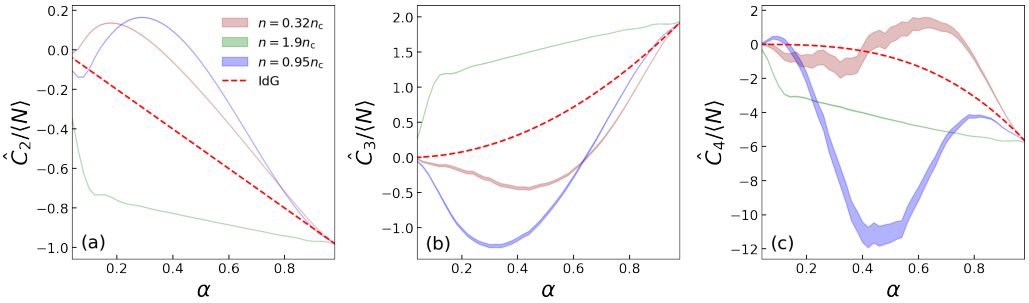

Figure 2. Normalized factorial cumulants as a function of acceptance α for three densities. $\hat{C}_4/\langle N\rangle$ demonstrates negative values with non-monotonic behavior as a CP signal.

6 Momentum Space Results

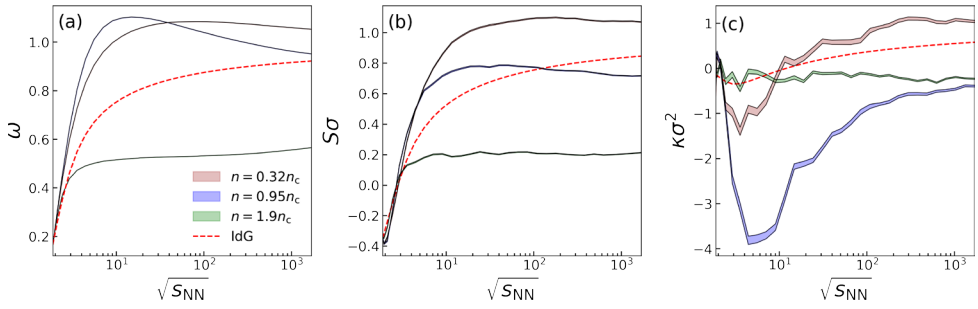

Figure 3. Momentum-space kurtosis as a function of $\sqrt{s_{\rm NN}}$ at $|y| < 0.5$ momentum cut with flow. A non-monotonic dip n ear $\sqrt{s_{\rm NN}} \approx 7.7$ GeV signals the CP.

Without flow, the cumulants match analytical ideal gas expectations in the momentum space ([9]). This gives us a motivation to introduce the Bjorken-like collective flow model

with freezeout temperature $T_{\rm frz} = 0.15$ GeV and $m_N = 0.938$ GeV

$$y_i = \frac{2\, y_{\rm beam}}{L}\, z_i + \sqrt{\frac{T_{\rm frz}}{m_N T}}\, v_{z,i}, \quad \text{where} \quad y_{\rm beam} = \ln\left[\frac{\sqrt{s_{\rm NN}} + \sqrt{s_{\rm NN} - 4m_N^2}}{2m_N}\right]. \tag{5}$$

This partially recovers the CP signals. At $n = 0.95 n_c$, momentum-space kurtosis dips near $\sqrt{s_{\rm NN}} \approx 7$ GeV (Fig. 3), and factorial cumulants mirror this trend, confirming the CP signal around this energy.

7 Conclusions

MD of the LJ fluid reveals strong CP signals in coordinate-space cumulants and factorial cumulants. Momentum-space analyses require collective flow to partially recover these non-Gaussian features. At momentum space with flow, strongest CP signal observed from $\sqrt{s_{\rm NN}} = 5$ to 10 GeV (Fig. 3). Interplay between acceptance size α and correlation from collective flow makes CP signal change non-monotonically. Future extensions include the partonic degrees of freedom, LJ virial EOS studies and realistic hydrodynamic expansion to better emulate heavy-ion collisions.

Acknowledgments

We thank Greg Morrison and Anar Rustamov for fruitful discussions. V.A.K. and V.V. acknowledge support from the University of Houston's Research Computing. V.A.K. and V.V. have been supported by the U.S. Department of Energy, Office of Science, Office of Nuclear Physics, Early Career Research Program under Award Number DE-SC0026065. V.K. has been supported by the U.S. Department of Energy, Office of Science, Office of Nuclear Physics, under contract number DE-AC02-05CH11231. M.I.G. is thankful for support from the Simons Foundation.

References

[1] A. Bzdak, S. Esumi, V. Koch, J. Liao, M. Stephanov and N. Xu, Mapping the Phases of Quantum Chromodynamics with Beam Energy Scan, Physics Reports, **853** (2020)

[2] Y. Hatta and M. Stephanov, Proton number fluctuation as a signal of the QCD critical endpoint, Phys. Rev. Lett. **91** 129901 (2003)

[3] M. A. Stephanov, K. Rajagopal and E. Shuryak, Event-by-event fluctuations in heavy ion collisions and the QCD critical point, Phys. Rev. D **60** 114028 (1999)

[4] V. Vovchenko, QCD at finite temperature and density: Criticality, EPJ Web Conf. **296** 01017 (2024)

[5] V. A. Kuznietsov. O. Savchuk, M. I. Gorenstein, V. Koch and V. Vovchenko, Critical point particle number fluctuations from molecular dynamics, Phys. Rev. C **105** 044903 (2022)

[6] V. Vovchenko, Molecular dynamics simulation and visualization of the Lennard-Jones system utilizing CUDA-enabled GPUs (GitHub repository), https://github.com/vlvovch/lennard-jones-cuda

[7] V. Vovchenko, O. Savchuk, R. V. Poberezhnyuk, M. I. Gorenstein and V. Koch, Connecting fluctuation measurements in heavy-ion collisions with the grand-canonical susceptibilities, Phys. Lett. B **811** 135868 (2020)

[8] A. Bzdak, V. Koch, J. Liao, and N. Strodthoff, Cumulants and correlation functions versus the QCD phase diagram, Phys. Rev. C, **95** (2017) M. P. Allen and D. J. Tildesley, Computer Simulation of Liquids, Oxford University Press (2017)

[9] Volodymyr A. Kuznietsov and Roman Poberezhniuk and Mark I. Gorenstein and Volker Koch and Volodymyr Vovchenko, High-order cumulants and correlation functions near the critical point from molecular dynamics, arXiv:nucl-th/2511.00755